ChemComm

Accepted Manuscript

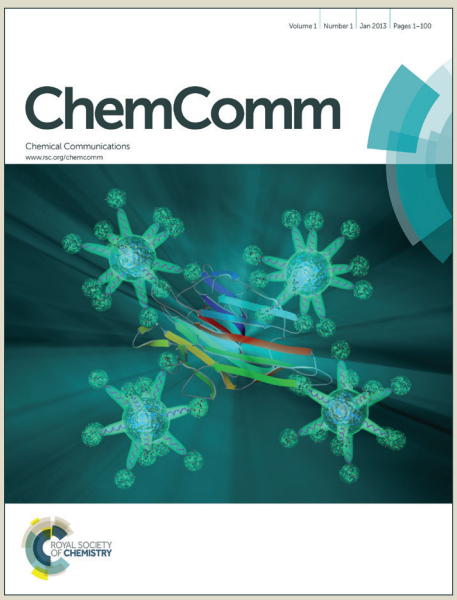

ROYAL SOCIETY OF CHEMISTRY

www.rsc.org/chemcomm

ChemComm

RSCPublishing

COMMUNICATION

Poring graphene to encapsulate $Na_{6.24}Fe_{4.88}(P_2O_7)_4$ as composite cathode materials for Na-ion batteries†

Cite this: DOI: 10.1039/x0xx00000x

Yubin Niu[a,b], Maowen Xu[a,b,*], Shu-Juan Bao[a,b] and Chang Ming Li[a,b,*]

Received 00th January 2012,
Accepted 00th January 2012

DOI: 10.1039/x0xx00000x

www.rsc.org/

$Na_{6.24}Fe_{4.88}(P_2O_7)_4$@pored graphene composite is fabricated as a cathode of Na-ion batteries for the first time by a hydrothermal-assisted sol-gel process. In comparison to non-pored composite and pristine ones, the as-prepared material exhibits much higher capacity and better rate, which are mainly attributed to graphene good conductivity and rational pored structure for significantly enhanced diffusion coefficient.

Compared with conventional oxide cathode material, polyanionic frameworks due to its excellent structural stability and voltage adjustable flexibility make it gain more and more attention whether in lithium or sodium ion batteries. To date, various polyanion-based cathode materials such as $Na_2Fe_2(SO_4)_3$[1], $Na_3V_2(PO_4)_3$[2-7], $NaFePO_4$[8], $Na_2FeP_2O_7$[9], $Na_2MnP_2O_7$[10], $Na_3M_2(PO_4)_2F_3$ (M = Ti, Fe, V)[11], $Na_3MPO_4CO_3$ (M = Fe, Mn, Co)[12-14], $Na_7V_4(P_2O_7)_4(PO_4)$[15, 16], $Na_2Fe_{3-x}Mn_x(PO_4)_3$[17], and $Na_4Fe_3(PO_4)_2(P_2O_7)$[18] have been extensively investigated. Unfortunately, most of them suffer from poor conductivity, which is generally crucial to performance[19], and relatively low capacity due to the presence of polyanion. Therefore, it is urgently needed to design and construct special structure with good conductivity, such as pore and multilayer structure combined with graphene, which may improve both high capacity and excellent rate performance.

In this communication, we construct porous $Na_{6.24}Fe_{4.88}(P_2O_7)_4$@porous graphene (labeled as NFPO@PG) composite, which exhibits higher capacity and better rate performance comparing with the pristine $Na_{6.24}Fe_{4.88}(P_2O_7)_4$ (labeled as NFPO) and $Na_{6.24}Fe_{4.88}(P_2O_7)_4$@graphene (labeled as NFPO@G). The precursor of the NFPO@PG composite was synthesized by using a hydrothermal-assisted sol-gel method. First, graphene oxide hydrogel was prepared from graphene oxide suspension by a hydrothermal method. The as-produced hydrogel was immersed into 50 mL ascorbic acid solution with vigorous and intense sonication process for 30 mins. Then, stoichiometric amounts of sodium acetate and ferrous chloride mixed solution was slowly added dropwise to the above solution with continuous stirring for 2 h at 70 ℃. Third, ammonium dihydrogen phosphate solution was added into the solution in sequence under constant stirring for 4 h at 70 ℃. After the water was removed by evaporation, the gel was frozen momentarily by slowly dropping into liquid nitrogen, and then the frozen solution was adopted by another vacuum drying process for 24 h in a freeze-drying machine. The obtained powders were ground in a mortar and heat-treated at 350 ℃for 6 h. Then, the powders were ground again in a mortar and annealed at 600 ℃ for 15 h under an argon atmosphere to obtain the final NFPO@PG composite. For comparison, a controlled NFPO and NFPO@G samples were also prepared, and the synthetic process was the same as mentioned above except for the hydrothermal process and freeze-drying process. Crystal structure of the obtained samples was characterized by powder X-ray diffraction (XRD, MAXima-X XRD-7000). Furthermore, the morphology and microstructure were examined by field-emission scanning electron microscopy (FESEM, JSM-6700F). For the electrochemical test, the cathode materials were evaluated in 2032 type coin cells using a Na disk as counter electrode and 1 M $NaClO_4$ in ethylene carbonate/diethyl carbonate (EC/DEC, 50 : 50 vol %) solution as electrolyte. The cathode film was prepared by mixing the composite material (85 wt %), acetylene black (10 wt%) and polyvinylidene fluoride (PVdF, 5 wt %) in N-methyl-pyrrolidinone (NMP) into an electrode slurry and then casting the slurry on aluminium foil collector and dried overnight in vacuum at 120 °C. The typical loading of the electroactive material per electrode was

approximately 1.1 mg. The assembly of the cells was carried out in a dry Ar-filled glove box. The galvanostatic charge-discharge tests were performed on a LAND cycler (Wuhan Kingnuo Electronic Co., China). Electrochemical impedance spectroscopy (EIS) experiments were conducted in the frequency range of 0.01-100 kHz with a CHI600D electrochemical analyzer.

NFPO crystallizes in a triclinic structure with *P-1* space group. Fig. 1a schematically shows that its framework is built on a centrosymmetrical crown of $Fe_2P_4O_{22}$ and $Fe_2P_4O_{20}$ moitiés connected by corner-sharing to form a three-dimensional framework. Each crown unit consists of two FeO_6 octahedra and two P_2O_7 groups. Fig. 1b presents the XRD patterns of as-prepared composite sample, which is consistent with the literature[20]. It should be noted that the crystallinity of the as-prepared materials is poor.

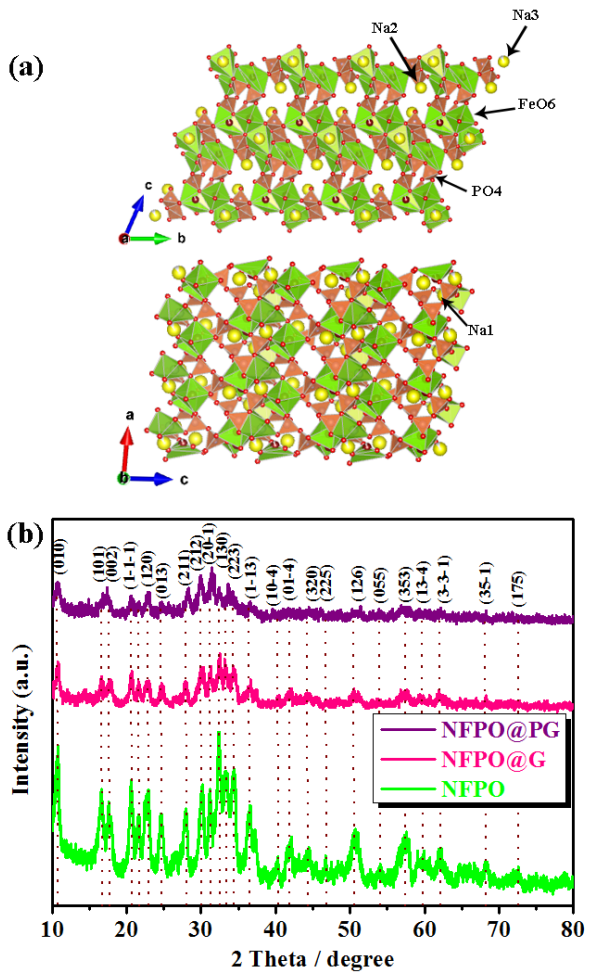

Fig. 1 (a) Crystal structure model of triclinic NFPO; (b) XRD patterns of as-prepared composite materials.

Fig. 2a, b and Fig. 2c, d show SEM images of NFPO@G and NFPO@PG, respectively. As seen from Fig. 2b and Fig. 2d, the particle size of them are less than 100 nm, and evenly distributed on graphene. However, compared with NFPO@G, a porous morphology is observed in NFPO@PG composite. Furthermore, this porous morphology and structure of the sample can be more clearly detected from Fig2d; the sample surface is rough and numerous pores are interconnected. The formation of this special porous structure is due to graphene oxide converted to graphene oxide hydrogel during the hydrothermal process. Meanwhile, the specific surface area and pore size distribution were used to investigate both NFPO@G and NFPO@PG (Fig. S1, ESI†) by using nitrogen isothermal adsorption-desorption measurement. Obviously, the specific surface area of the materials significantly increases from 12.04 m^2 g^{-1} (NFPO@G) to 57.00 m^2 g^{-1} (NFPO@PG) after pore-forming. It is thus expected that these porous morphologies are beneficial to the penetration of the electrolyte while enlarging the contact area between electrode and electrolyte, both of which be beneficial to the improvement of the electrochemical performance of the electrode materials. Moreover, the porous structure can reduce path lengths for Na^+ diffusion and increase specific capacities, particularly at high charge/discharge rates.[21] The carbon content in NFPO@PG is estimated from TG analysis to be approximately 5.3 wt% (Fig. S2, ESI †). TEM measurements were carried out to obtain knowledge of the structural and morphological evolution of the sample, Bright-field images of the samples reveal fine (～20 nm) crystalline NFPO (Fig. S3a and c, ESI†). HRTEM images in Fig. S3b and d show marked *d*-spacing of 0.821 nm, 0.204 nm and 0.245 nm corresponding well with that of (010), (320) and (134) planes of triclinic NFPO, respectively. These results are consistent with the XRD pattern obtained for these samples (Fig. 1b).

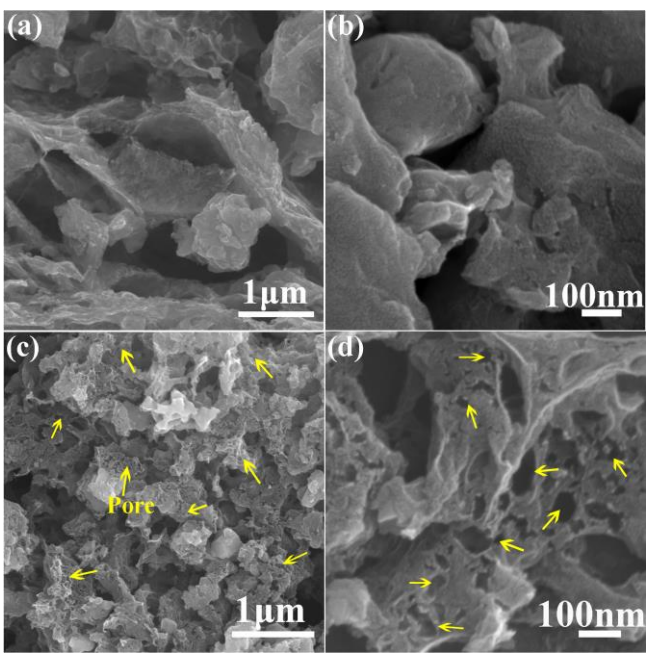

Fig. 2 SEM images of NFPO@G (a, b) and NFPO@PG (c, d).

Fig. 3a shows the cycling performance of the three composite materials at 0.2C. After 50 cycles, NFPO,

NFPO@G and NFPO@PG discharge a capacity of ~80 mAh g^{-1}, 106 mAh g^{-1} and 114 mAh g^{-1}, respectively, maintaining more than 95% of the initial values. In contrast, graphene composites have higher specific capacity and better cycling stability, hereinto, NFPO@PG has relatively higher capacity. Two mainly pair of oxidation (Na extraction) and corresponding reduction (Na insertion) peaks can be observed among the oxidation peaks located at 2.51, 2.98 V for NFPO@G and at 2.51, 2.94 V for NFPO@PG, and corresponding reduction peaks of 2.47, 2.90 V and 2.47, 2.92 V, respectively (Fig. 3b). Noticeably, the latter has smaller polarization (~0.02 V) in the second pair of redox peaks position. Fig. 3c compares the rate performance of NFPO@PG with those of NFPO and NFPO@G. Intuitively, the former exhibits an excellent discharge capability with the rate increases, implying the effectiveness of our strategy. It is worth noting that after the rate performance test, all of them have good capacity recovery capability at 0.2C, to some extent, which results from excellent structural stability of the polyanionic frameworks. Fig. 3d shows the corresponding typical discharge curves of NFPO@PG sample at rates from 0.2 to 3.2 C. Two mainly voltage plateaus can be observed, which are in good agreement with Fig. 3b.

The above assumption could be proved by EIS measurements obtained at 3.0 V and 3.2 C. The apparent diffusivity of Na^+ was further calculated to probe the effect of porous structure on the kinetics of NFPO@G electrodes. The computation was based on the following equation:

$$D_{Na^+} = \left(\frac{2RT}{\sqrt{2}n^2F^2\sigma_w AC}\right)^2 = \frac{2R^2T^2}{n^4F^4\sigma_w^2A^2C^2}$$

where R, T, A, F, n, C and σ_w are the gas constant, the absolute temperature, the surface area of the electrode, the Faraday´s constant, the number of electrons per molecule during oxidation, the Na^+ concentration in the cathode material, and the Warburg factor which is related to Z', respectively.

Fig. 3e shows the plots of Z' and $\omega^{-1/2}$ at low frequency, σ_w can then be explored from the slope of the fitting line. Compared with NFPO@G composite, the diffusion coefficient of sodium ion is about six times higher than that of NFPO@G. These results clearly suggest that the kinetics of NFPO@G is improved by constructing the pore structure.

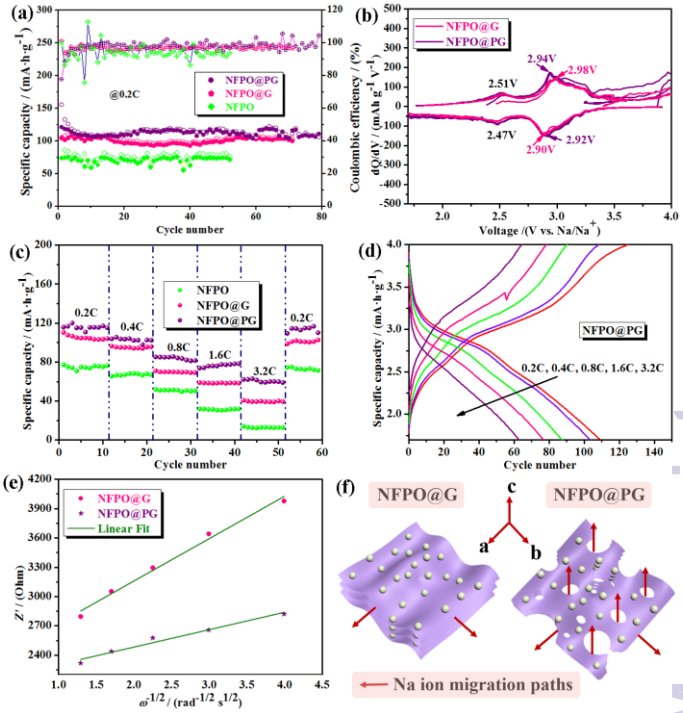

Fig. 3 (a) Galvanostatic charge-discharge cyclability at 0.2C and coulombic efficienecy; (b) chronoamperograms of the first three cycles corresponding with (a); (c) Performance of NFPO@G and NFPO@PG at various rates from 0.2C to 3.2C; (d) The charge-discharge curves of NFPO@PG at different rates; (e) Relationship between Z′ and $\omega^{-1/2}$ at low frequency calculated by EIS measurement obtained at 3.0 V and 3.2C; (f) Illustration of Na ion migration paths in electrolytes.

According to the present results here, Fig. 3f will intuitively show us the migration paths of Na^+ in electrolyte. Na ion diffusion only in two directions along a and b, namely 2D diffusion channel in NFPO@G composite, while there are three diffusion directions along a, b and c, namely 3D diffusion channel in NFPO@PG composite.

In summary, NFPO@PG composite was fabricated through the hydrothermal-assisted sol-gel method as a cathode material in Na-ion batteries, showing higher capacity and better rate performance comparing with NFPO and NFPO@G, NFPO@PG composite, mainly attributed to graphene excellent conductivity and pored structure for significantly enhanced diffusion coefficient. This approach holds great promise for a high performance cathode in Na-ion battery applications.

This work is financially supported by Chongqing Key Laboratory for Advanced Materials and Technologies of Clean Energies under cstc2011pt-sy90001, Start-up grant under SWU111071 from Southwest University and Chongqing Science and Technology Commission under cstc2012gjhz90002. The work is also supported by grants from Fundamental Research Funds for the Central Universities (SWU113079, XDJK2014C051) and Program for the Youth Talent in Science and Technology of Chongqing (cstc2014kjrc-qnrc50006)

Notes and references

a. Institute for Clean Energy & Advanced Materials, Faculty of Materials and Energy， Southwest University, Chongqing 400715, P.R. China.
b. Chongqing Key Laboratory for Advanced Materials and Technologies of Clean Energies, Chongqing 400715, P.R. China.
** Corresponding author*
E-mail: ecmli@swu.edu.cn or xumaowen@swu.edu.cn

1. P. Barpanda, G. Oyama, S.-i. Nishimura, S.-C. Chung and A. Yamada, *Nat Commun*, 2014, **5**.
2. Z. Jian, W. Han, X. Lu, H. Yang, Y.-S. Hu, J. Zhou, Z. Zhou, J. Li, W. Chen, D. Chen and L. Chen, *Adv. Energy Mater.*, 2013, **3**, 156-160.
3. Z. Jian, C. Yuan, W. Han, X. Lu, L. Gu, X. Xi, Y.-S. Hu, H. Li, W. Chen, D. Chen, Y. Ikuhara and L. Chen, *Adv. Funct. Mater.*, 2014, **24**, 4265-4272.
4. Z. Jian, L. Zhao, H. Pan, Y.-S. Hu, H. Li, W. Chen and L. Chen, *Electrochem. Comm.*, 2012, **14**, 86-89.
5. Y. H. Jung, C. H. Lim and D. K. Kim, *J. Mater. Chem. A*, 2013, **1**, 11350-11354.
6. S. Kajiyama, J. Kikkawa, J. Hoshino, M. Okubo and E. Hosono, *Chem.-Eur. J.*, 2014, **20**, 12636-12640.
7. J. Kang, S. Baek, V. Mathew, J. Gim, J. Song, H. Park, E. Chae, A. K. Rai and J. Kim, *J. Mater. Chem.*, 2012, **22**, 20857-20860.
8. M. Avdeev, Z. Mohamed, C. D. Ling, J. Lu, M. Tamaru, A. Yamada and P. Barpanda, *Inorg. Chem.*, 2013, **52**, 8685-8693.
9. P. Barpanda, G. Liu, C. D. Ling, M. Tamaru, M. Avdeev, S.-C. Chung, Y. Yamada and A. Yamada, *Chem. Mater.*, 2013, **25**, 3480-3487.
10. P. Barpanda, T. Ye, M. Avdeev, S.-C. Chung and A. Yamada, *J. Mater. Chem. A*, 2013, **1**, 4194-4197.
11. K. Chihara, A. Kitajou, I. D. Gocheva, S. Okada and J.-i. Yamaki, *J. Power Sources*, 2013, **227**, 80-85.
12. W. Huang, J. Zhou, B. Li, J. Ma, S. Tao, D. Xia, W. Chu and Z. Wu, *Sci. Rep.*, 2014, **4**.
13. H. Chen, Q. Hao, O. Zivkovic, G. Hautier, L.-S. Du, Y. Tang, Y.-Y. Hu, X. Ma, C. P. Grey and G. Ceder, *Chem. Mater.*, 2013, **25**, 2777-2786.
14. C. L. Wang, M. Sawicki, S. Emani, C. H. Liu and L. L. Shaw, *Electrochimica Acta*, 2015, **161**, 322-328.
15. C. Deng and S. Zhang, *ACS Appl. Mater. Interfaces*, 2014, **6**, 9111-9117.
16. C. Deng, S. Zhang and Y. Wu, *Nanoscale*, 2015, **7**, 487-491.
17. W. Huang, B. Li, M. F. Saleem, X. Wu, J. Li, J. Lin, D. Xia, W. Chu and Z. Wu, *Chem.-Eur. J.*, 2014, **21**, 851-860.
18. J. Y. Jang, H. Kim, Y. Lee, K. T. Lee, K. Kang and N.-S. Choi, *Electrochem. Comm.*, 2014, **44**, 74-77.
19. L. Zhao, J. Ni, H. Wang and L. Gao, *RSC Adv.*, 2013, **3**, 6650-6655.
20. K.-H. Ha, S. H. Woo, D. Mok, N.-S. Choi, Y. Park, S. M. Oh, Y. Kim, J. Kim, J. Lee, L. F. Nazar and K. T. Lee, *Adv. Energy Mater.*, 2013, **3**, 770-776.
21. W. Shen, C. Wang, H. Liu and W. Yang, *Chem.-Eur. J.*, 2013, **19**, 14712-14718.

